LANGMUIR Article
Cite This: Langmuir XXXX, XXX, XXX−XXX
pubs.acs.org/Langmuir

Robust and Biocompatible Functionalization of ZnS Nanoparticles by Catechol-Bearing Poly(2-methyl-2-oxazoline)s

Angela Federica De Fazio,[†,‡] Giulia Morgese,[§] Maddalena Mognato,[∥] Celeste Piotto,[∥] Danilo Pedron,[†] Gloria Ischia,[⊥] Valerio Causin,[†] Jan-Georg Rosenboom,[#] Edmondo M. Benetti,*[,§] and Silvia Gross*[,†]

[†]Dipartimento di Scienze Chimiche, Università degli Studi di Padova, via Marzolo 1, 35131 Padova, Italy
[‡]Physics and Astronomy, University of Southampton, Highfield Campus SO17 1BJ, Southampton, United Kingdom
[§]Polymer Surfaces Group, Laboratory for Surface Science and Technology, ETH Zürich, Vladimir-Prelog-Weg 5, 8093-CH Zürich, Switzerland
[∥]Dipartimento di Biologia, Università degli Studi di Padova, via U. Bassi 58/B, 35131 Padova, Italy
[⊥]Dipartimento di Ingegneria Industriale, Università di Trento, via Sommarive 9, 38122 Trento, Italy
[#]Department of Chemistry and Applied Biosciences, Institute of Chemical and Bioengineering, ETH Zürich, Vladimir-Prelog-Weg 1-5/10 8093 Zürich, Switzerland

Supporting Information

ABSTRACT: Zinc sulfide (ZnS) nanoparticles (NPs) are particularly interesting materials for their electronic and luminescent properties. Unfortunately, their robust and stable functionalization and stabilization, especially in aqueous media, has represented a challenging and not yet completely accomplished task. In this work, we report the synthesis of colloidally stable, photoluminescent and biocompatible core−polymer shell ZnS and ZnS:Tb NPs by employing a water-in-oil miniemulsion (ME) process combined with surface functionalization via catechol-bearing poly-2-methyl-2-oxazoline (PMOXA) of various molar masses. The strong binding of catechol anchors to the metal cations of the ZnS surface, coupled with the high stability of PMOXA against chemical degradation, enable the formation of suspensions presenting excellent colloidal stability. This feature, combined with the assessed photoluminescence and biocompatibility, make these hybrid NPs suitable for optical bioimaging.

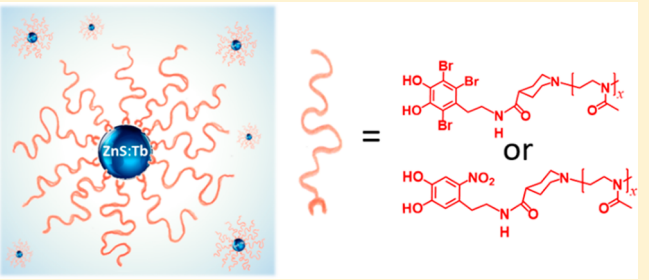

INTRODUCTION

The robust, steric stabilization of inorganic nanoparticles (NPs) within aqueous and physiological media via an appropriate chemical functionalization stands as a fundamental requirement to enable their application in the biomedical field. Whereas in the cases of metallic and metal oxide NPs well-established and reliable functionalization protocols have been set,[1] the development of effective surface-derivatization methods for metal sulfide-based analogues has not been achieved so far by synthetic chemists, and, in particular, the actual chemical nature of the functionalized surface has not been thoroughly characterized.[2] Furthermore, reports retrieved in the literature fail to convincingly demonstrate the stable functionalization of metal sulfides.[3,4]

Zinc sulfide (ZnS) has been especially investigated, because of its appealing electronic properties, i.e., a wide band gap (3.7 eV) and a high exciton binding energy (40 meV).[5,6] These features make ZnS one of the most appealing semiconducting materials for the fabrication of electroluminescent devices, allowing a direct conversion of electric energy into visible light, without generating heat or requiring chemical or mechanical triggers.[7] In addition, ZnS can be accessibly doped by multiple ions (multiplexing), making it a suitable starting material for the development of optical and optoelectronic devices.[7]

For all these reasons, combined with their nontoxicity and intrinsic photoluminescence, ZnS NPs are envisioned as high-performing and biocompatible bioimaging probes.[4,8]

Despite their appealing properties, a comprehensive and unambiguous characterization of the surface composition of ZnS NPs (following the diverse synthetic pathways to obtain them) has not been provided so far,[9−11] thereby hampering the identification of an effective functionalization protocol and making the choice of a robust anchoring chemistry a challenging task. Although, in several experimental and theoretical studies, it has been proposed that the ZnS surface could feature either oxidized species (SO_4, SO_3, ZnO) or reduced (SH, ZnOH) moieties,[12] no unequivocal proof of the chemical nature of these surfaces has been presented yet. Hence, coherent evidence of the selective ZnS surface

Received: July 6, 2018
Revised: August 22, 2018
Published: August 31, 2018

derivatization by adsorbates presenting appropriate organic anchors still remains a partially unaccomplished issue.

Recently, the incorporation of ZnS:Mn NPs into a polymeric matrix including poly(acrylic acid) (PAA) and poly(methyl methacrylate) (PMMA) to convey luminescent properties to plastics was investigated, although no specific functions of the polymers were demonstrated to enhance the interactions with the NPs.[13,14] Alternatively, semiconductor nanocrystals (entirely or partially constituted by sulfides[15,16]) were successfully incorporated into polymeric matrices[14,17] or derivatized with oleic acid and hexadecyl-trimethylammonium bromide[18] to permit their dispersion in organic phases. Also in these cases, no detailed description of the characteristics of the coated surface and proofs of the effective functionalization were provided.

In several other reports,[3,19,20] the functionalization of ZnS NPs was achieved by means of adsorbates presenting cysteine functions, suggesting the formation of S−S linkages with the sulfur present on the NP surface. Remarkably, the stability of the obtained suspensions was not addressed. More recent reports[21,22] focused on ZnS:Mn quantum dots coated with pyridine or hypromellose, where these capping agents were loaded during the ZnS:Mn quantum dots synthesis and acted as both stabilizing and growth-inhibitor agents. The successful surface derivatization was verified by Fourier transform infrared (FT-IR) spectroscopy.

Motivated by the need to find suitable and effective adsorbates for the stable functionalization and dispersion of ZnS NPs in aqueous media, we especially focused on the development of poly(2-methyl-2-oxazoline) (PMOXA)-based ligands. The application of PMOXA for NPs stabilization represents a technologically relevant strategy for further biomedical applications,[23−34] as PMOXA proved to be more chemically stable toward oxidation and enzymatic degradation, compared to the most applied poly(ethylene glycol) (PEG) derivatives, yet maintaining good biocompatibility and endowing the NPs with stealth properties.[35−37] In particular, we first synthesized ZnS and Tb-doped ZnS (ZnS:Tb) NPs by a miniemulsion (ME) approach,[38] obtaining discrete aggregates of NPs with typical crystallite dimensions of 6 nm. The structure and the surface composition of the NPs were characterized by a combination of X-ray photoelectron spectroscopy (XPS), powder X-ray diffraction (XRD), and transmission electron microscopy−selected area electron diffraction (TEM-SAED), which consistently indicated the presence of crystalline sphalerite ZnS. Later, PMOXA bearing substituted catechol end-groups were anchored to the NPs. Similar functions were previously shown to enable the functionalization of different metal oxide NPs, including Fe_3O_4 and ZnO, through the formation of a stable five-membered coordination ring with the metal centers exposed at the NPs surface.[35,39−41] In the present study, we demonstrate that nitrodopamine (ND) and bromo-substituted dopamine (BrD) can effectively bind to the ZnS surface, forming a densely grafted polymer shell. The substitution of catechol-based anchors with electron-withdrawing groups, such as NO_2 and Br, decreases the pK_a of the hydroxyl moieties. This provides a stronger binding to the metal surface, when compared to unmodified catechols, and simultaneously prevents the catechol self-polymerization/oxidation reactions.[40,42] These features are especially remarkable for the functionalization of ZnS NPs. On the one hand, the lower acidity of the Zn^{2+} in ZnS, with respect to ZnO, can be partially compensated by the enhanced reactivity of the substituted catechols, on the other hand, the stronger affinity of the ligands toward the ZnS surface inhibits its oxidation or passivation.

Relevantly, ND and BrD anchors feature a similar affinity toward the inorganic surface; however, they present different optical properties, with the former adsorbing in the near UV and thus presenting some limitations when bioimaging applications or staining procedures are required.

Investigating a selection of PMOXAND and PMOXABrD for the functionalization of ZnS and ZnS:Tb NPs, the molar mass of the ligand emerges as a key parameter for ensuring the long-term steric stabilization of the colloids against aggregation and Ostwald ripening in physiological media.

Finally, the luminescent properties of Tb-doped NPs were assessed and the biocompatibility of the fabricated ZnS-PMOXAs and ZnS:Tb-PMOXAs hybrids was tested on human lung adenocarcinoma (A549 cell line) cells, showing absence of cytotoxicity, and disclosing exciting perspectives for the application of these NPs as optical bioimaging probes.

EXPERIMENTAL SECTION

Materials. For the preparation of ZnS NPs, zinc nitrate hexahydrate ($Zn(NO_3)_2{\cdot}6H_2O$) and sodium sulfide (Na_2S) were obtained from Sigma−Aldrich, cyclohexane (C_6H_{12}) was purchased from Alfa−Aesar. The polyglycerol polyricinoleate (PGPR) was obtained from Palsgaard. All chemicals were used without further purification. For the synthesis of PMOXA ligands, all the chemicals were purchased from Aldrich. 2-Methyl-2-oxazoline (MOXA) and methyl triflate (MeOTf) were distilled over KOH and CaH_2, respectively, before use.

Preparation of ZnS Nanoparticles (NPs). Two identical mixtures, A and B, were prepared by dispersing PGPR (0.16 g) in cyclohexane (16 g); then, 3 g of an aqueous 0.5 M solution of $Zn(NO_3)_3$ (0.8 mmol, 2 mL) were added to mixture A and mechanical stirring allowed us to yield emulsion A′. Emulsion B′ was obtained by adding 3 g of an aqueous 1 M solution of Na_2S (2.8 mmol, 2.8 mL) to mixture B and subsequent mechanical stirring. Corresponding miniemulsions A and B were obtained by ultrasonication performed at the same time (3 min) and amplitude, by using a homogenizer (Sartorius Stedim LabsonicP) equipped with a titanium tip of 3 mm in diameter, working at an amplitude of 70% (corresponding to an acoustical power of 322 W cm^{-2}). A and B were mixed together and sonicated for the same time and at the same amplitude. The resulting white miniemulsion was mechanically stirred at room temperature for 4 h. Then, the powder product was separated by centrifugation (10 000 rpm, 10 min) and washed with acetone and deionized water several times. The white solid was dried in an oven at 80 °C for 4 h. In the case of the Tb-doped ZnS NPs, a similar procedure was followed, adding $Tb(NO_3)_3$ to solution A (1:20 w/wwith respect to $Zn(NO_3)$) (see Figure S1 in the Supporting Information).

Nitrodopamine Hemisulfate and Tribromodopamine Hydrobromide. Nitrodopamine hemisulfate was synthesized according to the literature.[43] The synthesis of tribromodopamine hydrobromide was performed according to previous reports.[44,45]

PMOXAND and PMOXABrD. COOH-terminated PMOXAs were synthesized according to a modification of a previously reported procedure.[30] MOXA (10, 20, 40, and 70 equiv, depending on DP) was dissolved in 30 mL of dry acetonitrile. MeOTf (1 equiv) was added at 0 °C to the monomer mixture. The polymerization was performed at 70 °C. After 24 h, ethylisonipecotate (3 equiv, distilled under vacuum) was added at room temperature (RT) and it was allowed to react for 48 h. The solution was dried under reduced pressure and the solid was dissolved in Milli-Q water, purified via dialysis, and finally lyophilized. Hydrolysis of ethyl-ester function at PMOXA chain ends was performed in NaOH aqueous solution (pH

DOI: 10.1021/acs.langmuir.8b02287
Langmuir XXXX, XXX, XXX−XXX

13) for 24 h. Purification and drying were performed via dialysis and freeze-drying. In order to obtain the catechol-bearing polymers, the polymer was dissolved in anhydrous dimethyl formamide (DMF) and two DMF solutions of N-hydoxysuccinimide (NHS) and N,N'-dicyclohexylcarbodiimide (DCC) were added separately to the polymer. After 24 h of stirring at RT, the catechols (ND or BrD) and *N*-methylmorpholine were added at 0 °C for additional 24 h. The purification first involved the filtration of the side-product dicyclohexylurea and then dialysis against water. The product was finally freeze-dried (see Figure S2 in the Supporting Information). Size exclusion chromatography (SEC) and ^{1}H nuclear magnetic resonanace (^{1}HNMR) spectroscopy were used to characterize PMOXAND and PMOXABrD ligands (see Table S1 and Figures S3−S7 in the Supporting Information).

ZnS NPs Functionalization. A DMF solution of the polymer was added to a suspension of ZnS in DMF (ZnS:polymer weight ratio = 1:50). The mixture was left to react overnight at RT. Then, the solution was dried and the solid suspended in Milli-Q water, purified by dialysis (membranes cutoff: 25 kDa), and finally freeze-dried.

XPS. Powder samples were investigated by XPS using a Perkin−Elmer φ 5600ci instrument with standard Al Kα radiation (1486.6 eV) operating at 350 W. The working pressure was lower than 5×10^{-8} Pa. The calibration was based on the binding energy (BE) of the Au $4f_{7/2}$ line at 83.9 eV, with respect to the Fermi level. The standard deviation for the BE values was 0.15 eV. Reported BEs were corrected for charging effects, and the BE value of 284.6 eV was assigned to the C 1s line of carbon. Survey scans were obtained in the 0−1350 eV range (pass energy = 187.5 eV, 1.0 eV step^{-1}, 25 ms step^{-1}). Detailed scans (pass energy = 29.35 eV, 0.1 eV step^{-1}, 50−150 ms step^{-1}) were recorded for the O 1s, C 1s, Zn 2p, ZnLMM, S 2p, and the Tb 3d regions. The atomic composition, after a Shirley-type background subtraction, was evaluated using sensitivity factors supplied by Perkin−Elmer. Peak assignment was performed according to literature data.[46−48]

X-ray Diffraction (XRD). The XRD patterns on the ZnS NPs were collected with a Bruker D8 Avance diffractometer that was equipped with a Göbel mirror by using the Cu Kα radiation in the 2θ range of 10°−70°. The angular accuracy was 0.001°, and the angular resolution was better than 0.01°.

Thermogravimetric Analysis (TGA). TGA measurements on the functionalized NPs were performed with a thermobalance LabSys Setarm SDT 2960 (TA Instruments) in the temperature range of 20−800 °C in air with a dynamic heating rate of 10 °C min^{-1}.

Transmission Electron Microscopy (TEM). TEM analysis was performed with a Philips CM12 microscope operating at 120 keV and equipped with an energy-dispersive X-ray spectroscopy (EDXS) system, which allowed for localized chemical analyses. For each sample, both images and SAED patterns were collected to investigate the morphology and dimensions of ZnS NPs, and their local chemical composition. For the identification of the phases and assignment of the relevant peaks, Process Diffraction software was used.

Atomic Force Microscopy (AFM). A Bruker Dimension Icon atomic force microscope was used in tapping mode, employing a SiN cantilever with a resonance frequency of 300 kHz, and the spring constant was 22.9 N m^{-1}.

Fourier Transform Infrared (FT-IR) Analysis. Experiments were performed on a NEXUS 870 FT-IR (Nicolet), operating in the transmission range of 400−4000 cm^{-1}, collecting 64 scans with a spectral resolution of 4 cm^{-1}. The measurements were recorded by dispersing the powders in anhydrous KBr pellets.

Size Exclusion Chromatography (SEC). Number- and weight-average absolute molecular weights (M_n and M_w, respectively) of PMOXA ligand precursors were determined by SEC. An Agilent 1100 unit was used; it was equipped with two PFG linear M columns (PSS) connected in series with an Agilent 1100 VWD/UV detector operated at 290 nm, a DAWN HELEOS 8 multiangle laser light scattering (MALS) detector (Wyatt Technology Europe), followed by an Optilab T-rEX RI detector from Wyatt. Samples were eluted in hexafluoroisopropanol (HFIP) with 0.02 M K-TFAc at 1 mL/min at room temperature. Absolute molecular weights were evaluated with Wyatt ASTRA software and dn/dc values based on our analytical setup (dn/dc (PMOXA) = 0.2498 mL/g).

Nuclear Magnetic Resonance (NMR). ^{1}H NMR spectra were collected on Bruker Ultrashield MHz 300 or 500 spectrometers in D_2O.

Dynamic Light Scattering (DLS). Dynamic light scattering (DLS) analysis on the suspensions were performed in water and PBS, using a Malvern Zetasizer NanoS, at a temperature of 20 °C.

Fluorescence Spectroscopy. Luminescence measurements were performed with a Horiba FluoroMax-P spectrofluorometer with a phosphorimeter accessory. The accuracy of the emission spectra was 0.5 nm.

Cell Culture. The human A549 cells (lung adenocarcinoma) were purchased from American Type Culture Collection (ATCC n. CCL-185) and cultured in Ham's F12-K Nutrient Mixture (Invitrogen Life Technologies, Carlsbad, CA, USA) supplemented with 10% heat inactivated fetal bovine serum (FBS, BIOCHROM, Berlin, Germany), 38 units/mL streptomycin, and 100 units/mL penicillin G, in T75 cm2 flasks (FALCON). Cells were kept at 37 °C in a humidified atmosphere of 95% air and 5% CO_2, and maintained in exponential and asynchronous phase of growth by repeated trypsinization and reseeding prior to reaching subconfluency. The cells were seeded and maintained for 24 h in complete culture medium before starting the NP treatment; then, the cells were incubated with medium (3% FBS) in which the NPs stock suspensions were freshly diluted. The percentage of serum (3%) supplemented represents the lower percentage suitable for maintaining the cells up to 72 h without suffering, in accordance with our previous observations.[49,50] Cells were incubated for 24 h with increasing concentrations of NPs (0.01−0.1 mg/mL) and then plated for clonogenic assay. Control cells underwent the same steps of treated cells, except for NPs exposure. For cytotoxicity analysis, the NPs stock solutions were diluted with ultrapure water (1 mg/mL) and the NPs suspensions were sterilized by filtration with 0.22 μm.

Clonogenic Assay. Cells (0.15×10^6/well) were seeded in 24-well plates and 24 h later were subjected to NPs treatment, harvested by trypsinization, and counted by Trypan Blue dye exclusion. Five hundred (500) viable cells were plated in 6 cm culture dishes in culture medium supplemented with 10% FBS and after 7−10 days at 37 °C, the colonies were counted after staining with 0.4% crystal violet and counted. Only colonies containing more than 50 cells were scored as survivors to determine the cloning efficiency (CE), i.e., the proportion of cells that attach and grow to the number of cells originally plated, expressed as a percentage. Cell survival was calculated as percentage of CE of NP-treated cells over that of untreated control cells.

Cellular Internalization of NPs. A549 cells (10^5) were seeded in 35 mm culture dishes and, after 24 h, were treated with NPs for 24 h. The cells seeded on a cover slip were primary fixed in 2.5% glutaraldehyde in 0.1 M sodium cacodylate buffer at pH 7.4 for 1 h at room temperature and then washed thrice with cacodylate buffer (10 min each wash). The samples were post-fixed with a mixture of 1% osmium tetroxide and 1% potassium ferrocyanide in 0.1 M sodium cacodylate buffer for 1 h at 4 °C, dehydrated in ethanol from 25% to 100% (thrice) for 10 min each step, and finally included in epoxy resin. The samples were sectioned with an Ultrotome V ultra-microtome (LKB instruments, Victoria, TX, USA). Thin sections (80−100 nm) were counterstained with uranyl acetate and lead citrate and then observed with a Tecnai G2 transmission electron microscope (FEI Company, Hillsboro, OR, USA) operating at 100 kV. Images were captured with a Veleta (Olympus Soft Imaging System) digital camera.

RESULTS AND DISCUSSION

Synthesis and Characterization of ZnS NPs. ZnS and ZnS:Tb NPs were synthesized following an inverse (water-in-oil, w-o) ME route, which afforded good control and reproducibility over the NP size.[38] A ME is a three-component metastable system composed by small droplets stabilized with

DOI: 10.1021/acs.langmuir.8b02287
Langmuir XXXX, XXX, XXX−XXX

Scheme 1. Preparation of ZnS and ZnS:Tb NPs via Miniemulsion (ME)[a]

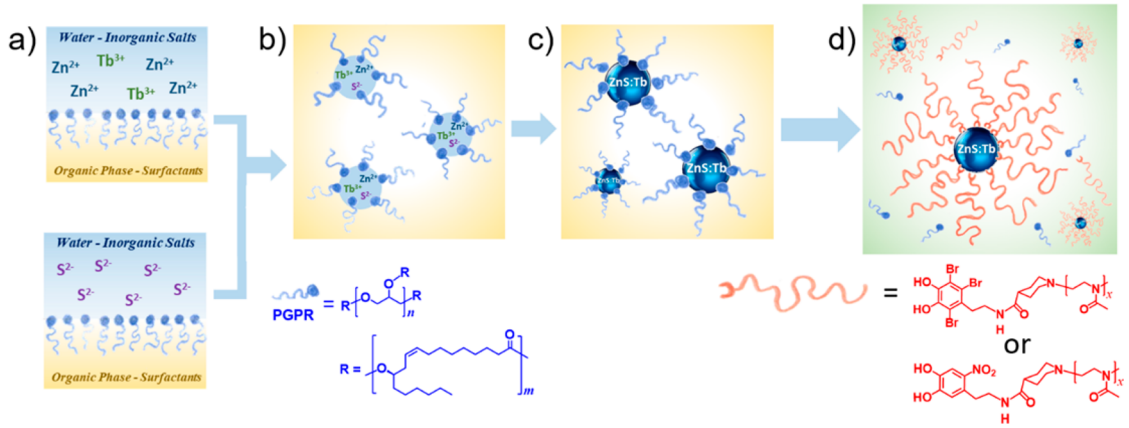

[a]Two aqueous solutions of metal and sulfide precursors were dispersed in cyclohexane (panel (a)), using polyglycerol polyricinoleate (PGPR) as an emulsifier (panel (b)). The formation of the NPs (panel (c)) was followed by the ligand exchange between PGPR and PMOXA ligands, to yield the desired ZnS-PMOXA and ZnS:Tb-PMOXAs core−polymer shell NPs (panel (d)).

a surfactant in an immiscible phase.[51−54] These systems have already been exploited for the crystallization of inorganic colloids.[46−55] Each droplet works as an independent nanoreactor in which the precipitation and the crystallization of the product occur already at RT.[38,56−58] Specifically, the preparation of ZnS NPs was achieved by mixing two aqueous solutions of $Zn(NO_3)_2$ and Na_2S, dispersed in cyclohexane, and using polyglycerol polyricinoleate (PGPR) as an emulsifier (see Scheme 1). This surfactant allowed us to achieve a hydrophilic/lipophilic balance (HLB) value in the range of 1−5, which is considered the optimum for the stabilization of w-o ME.[58]

The crystalline structure of the synthesized NPs was verified by XRD. The typical diffraction pattern displayed in Figure 1

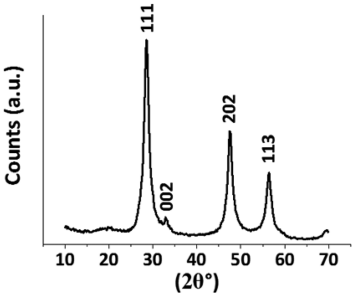

Figure 1. XRD pattern of ZnS NPs.

evidences the formation of crystalline ZnS as sphalerite polymorph already at RT (PDF N. 00-001-1281, 2θ = 28.55, 32.95, 47.55, 56.45), without the need of further thermal treatment.[38] An average crystallite size of 6 nm was determined by applying the Scherrer equation.[59]

The chemical composition of the surface of the NPs was subsequently analyzed by XPS (Figure 2). The survey spectrum, covering the entire BE range (0−1350 eV), revealed all the species of interest (S, Zn, O, C) (Figure 2a). The peaks corresponding to carbon and oxygen were mainly due to the presence of PGPR surfactant physisorbed on the surface of the NPs, as well as to adventitious contamination. XPS investigation was deepened by recording more-detailed spectra within narrower BE regions. From the Zn 2p and S 2p XPS regions (see Figures 2b and 2c), it was possible to determine

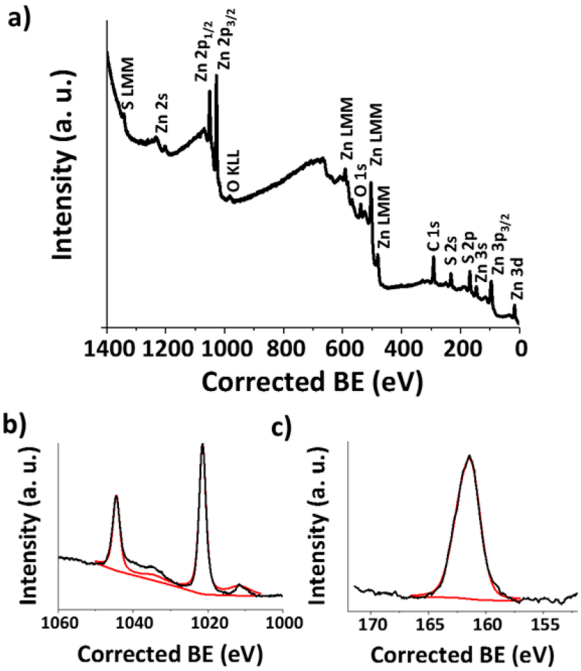

Figure 2. (a) XPS survey spectrum of ZnS NPs; (b, c) detailed spectra of the Zn 2p (panel (b)) and S 2p region (panel (c)).

the binding energies and atomic concentrations (percentage) of the species on the exposed surface of the NPs.

In order to rule out the presence of a $ZnSO_4$ passivating layer on the NPs, the oxidation state and chemical environment of sulfur and zinc were evaluated by fitting the S 2p and Zn 2p signals. The S 2p peak should be a doublet but, given the low resolution of the spectrometer (0.15 eV) and the low value of the spin−orbit splitting (1.18 eV),[60] this could not be evidenced. This signal was fitted with a single interpolation peak, showing that all the S-containing species at the surface of the NPs have the same chemical environment. The BE for the transition corresponded to 161.5 eV, which is compatible with S in ZnS.[61] The presence of $ZnSO_4$ could be excluded, as the typical binding energies for this compound would be expected in the range of 169.2−169.8 eV for S 2p[60,61] and at ∼1023 eV for Zn $2p_{3/2}$. Further evidence for the presence of ZnS at the

DOI: 10.1021/acs.langmuir.8b02287
Langmuir XXXX, XXX, XXX−XXX

surface of NPs was the measured BE for Zn, which was compatible with those reported for ZnS.[60] Finally, the quantitative analysis confirmed an atomic ratio Zn:S of 1:1, which is consistent with the stoichiometry of ZnS.

The absence of metal oxide species on the surface of NPs was further corroborated via SAED, which was performed on TEM micrographs (see Figures 3a and 3b). As shown in Figure 3a, ZnS NPs present an average diameter of ∼10 nm, in good agreement with the value obtained by the Scherrer equation. Remarkably, the diffraction pattern associated with the SAED analysis was indexed as ZnS and no presence of ZnO could be highlighted (Figure 3b). Hence, the combination of XPS, XRD, and SAED data unambiguously demonstrated that the inverse ME process yielded NPs exclusively featuring ZnS at their exposed surface.

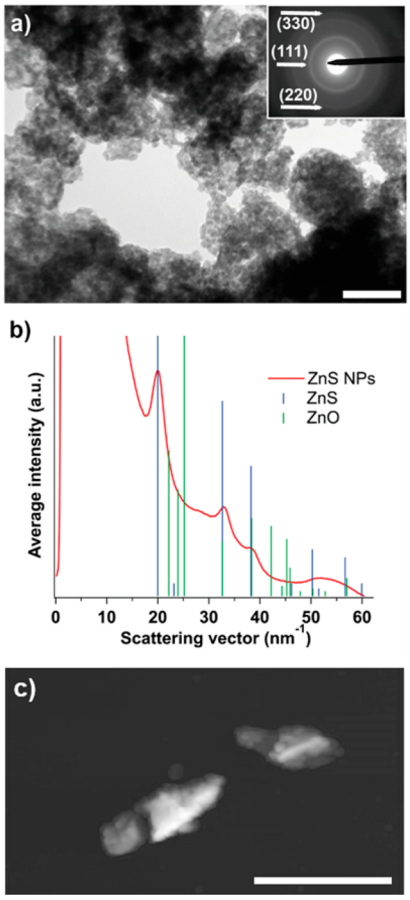

Figure 3. (a) TEM micrograph and SAED pattern of pristine ZnS NPs. Scale bar = 50 nm. (b) Integrated diffraction pattern of ZnS NPs as synthesized. The red trace is the experimental average intensity over circles, the blue and green set of signals are namely the tabulated ZnS (PDF No. 01-0792) and ZnO (PDF No. 79-2205). (c) Atomic force microscopy (AFM) tapping-mode micrograph highlighting aggregates of pristine ZnS NPs (the scale bar corresponds to 1 μm).

Synthesis and Characterization of ZnS-PMOXA NPs. PMOXA ligands with different molar masses and presenting either ND or BrD chain ends were applied as surface modifiers and stabilizers for ZnS NPs. Four different carboxylic acid-terminated PMOXAs, presenting average molar masses of 1500, 2300, 4500, and 8000 Da, were synthesized corresponding to average degrees of polymerization (DP) of 18, 27, 50 and 90, respectively (a detailed characterization of PMOXA species is reported in the Supporting Information). The different polymers were subsequently coupled to ND hemisulfate or BrD hydrobromide salts via NHS/DCC chemistry (see the Experimental Section and Figures S2−S8 in the Supporting Information for details), finally yielding eight different ligands, PMOXA(18)ND, PMOXA(27)ND, PMOXA(50)ND, PMOXA(90)ND, PMOXA(18)BrD, PMOXA(27)BrD, PMOXA(50)BrD, and PMOXA(90)BrD. The two types of anchors used in this study, ND and BrD, feature different light adsorption properties (see Figure S9 in the Supporting Information), which make them interesting compounds for the designing of hybrid materials for optical bioimaging.

ZnS and ZnS:Tb NPs were functionalized with the different PMOXA(x)ND and PMOXA(x)BrD by direct ligand exchange, suspending the PGPR-stabilized NPs in DMF in the presence of a 50-fold weight excess of each PMOXA ligand. After purification via dialysis, ZnS-PMOXA(x)ND and ZnS-PMOXA(x)BrD were collected.

Because of the stronger affinity of the catechol anchors for the ZnS surface compared to the surfactants physisorbed during the ME synthesis, a nearly quantitative functionalization was achieved. As exemplarily shown in Figure 4, the FT-IR spectra of ZnS-PMOXA(90)ND and ZnS-PMOXA(50)BrD NPs suspensions displayed the typical signals ascribable to the PMOXA ligand at 1637 cm^{-1} (amide C═O stretching) and between 1480 and 1400 cm^{-1} (polymeric CH bending and aromatic C═C stretching). Simultaneously, the signals characteristic of the PGPR surfactant (carbonyl vibrations at 1731 cm^{-1} and ether stretching at 1200 cm^{-1}) disappeared, indicating the successful and quantitative ligand exchange.

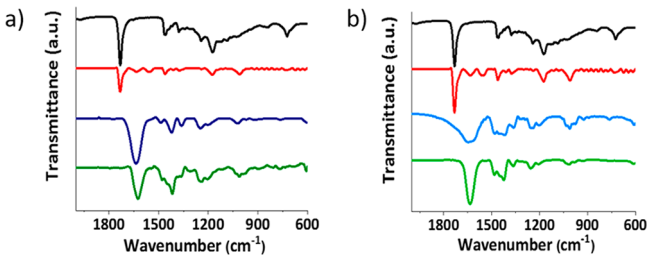

Figure 4. (a) FT-IR spectra of PGPR surfactant (black trace), PGPR-stabilized ZnS NPs (red trace), PMOXA(90)ND (blue trace), and ZnS-PMOXA(90)ND (green trace). (b) FT-IR spectra of PGPR surfactant (black trace), PGPR-stabilized ZnS NPs (red trace), PMOXA(50)BrD (blue trace), and ZnS-PMOXA(50)BrD (green trace).

The functionalization of ZnS NPs by the different PMOXA ligands was additionally evaluated by thermogravimetric analysis (TGA) (Figure S10 in the Supporting Information). Specifically, TGA measurements were performed to estimate the amount of ligand bound to the NPs after ligand exchange and purification by dialysis. The weight fraction of bound ligand obtained by TGA was compared for each sample with the initial PMOXA weight fraction introduced during the ligand exchange (both quantities are expressed, in terms of weight percent, in Table 1). The results showed that all the different PMOXA ligands quantitatively bound the surface of ZnS NPs until surface saturation was achieved, confirming the effective and quantitative functionalization of ZnS NPs by catechol-substituted PMOXAs. In all the cases, the PMOXA:ZnS weight ratio used for the ligand exchange was 50:1,

DOI: 10.1021/acs.langmuir.8b02287
Langmuir XXXX, XXX, XXX−XXX

Table 1. TGA of ZnS-PMOXAs NPs, Initial Weight Percentage of PMOXA Added during Ligand Exchange, and Weight Percentage of Bound PMOXA

	PMOXA Amount (wt %)	
sample	initial	bound
ZnS-PMOXA(18)BrD	98	90
ZnS-PMOXA(27)BrD	98	92
ZnS-PMOXA(50)BrD	98	93
ZnS-PMOXA(90)BrD	98	97
ZnS-PMOXA(18)ND	98	92
ZnS-PMOXA(27)ND	98	95
ZnS-PMOXA(50)ND	98	90
ZnS-PMOXA(90)ND	98	92

corresponding to 98% PMOXA. The amount of polymer ligand applied thus exceeded NPs surface saturation, which was reached at PMOXA:ZnS weight ratios ranging from 90% to 97%.

The amount of bound polymer measured by TGA could be used to estimate the surface density of PMOXA ligands, which was always included between 2 chains nm^{-2} and 6 chains nm^{-2}, in accordance to the values previously reported for chemically similar polymer shells on metal oxide NPs.[36]

The stability of ZnS-PMOXA NPs dispersions was subsequently monitored in water and in PBS at pH 7.4 by DLS (see Table 2), recording the average hydrodynamic diameter (HD) of the dispersed NPs over a period of 7 days (see Figure S11 in the Supporting Information).

Table 2. Average Hydrodynamic Diameters (HD) of ZnS-PMOXA NPs (in water and PBS), Determined by DLS Analysis

	Average HD - Intensity Distribution[a] (nm)	
sample	in water	in PBS
ZnS-PMOXA(18)ND	200 ± 110 (100%)	298 ± 131 (70%)
		191 ± 170 (30%)
ZnS-PMOXA(18)BrD	146 ± 4 (99%)	570 ± 213 (100%)
ZnS-PMOXA(27)ND	139 ± 18 (60%)	216 ± 40 (65%)
	3.5 ± 0.2 (36%)	3.2 ± 0.6 (25%)
ZnS-PMOXA(27)BrD	131 ± 6 (100%)	132 ± 5 (100%)
ZnS-PMOXA(50)ND	162 ± 6 (100%)	159 ± 3 (100%)
ZnS-PMOXA(50)BrD	145 ± 4 (100%)	145 ± 4 (100%)
ZnS-PMOXA(90)ND	152 ± 4 (100%)	146 ± 4 (99%)
ZnS-PMOXA(90)BrD	155 ± 6 (100%)	153 ± 7 (100%)

[a]Area percentages are reported in brackets.

PMOXA ligands with relatively low DP (PMOXA(18) and PMOXA(27)) were less effective in stabilizing the NPs, particularly in PBS, where the formation of large aggregates was recorded.

In contrast, the longer PMOXA(50) and PMOXA(90) provided stable suspensions with average HD values ranging between 145 nm and 165 nm. Especially in PBS, where the presence of electrolytes reduces the electrostatic repulsions between NPs and thins the electrical double layer, high-molar-mass PMOXA ligands efficiently prevented aggregation and flocculation of the NPs. Moreover, it is important to emphasize that aqueous dispersions of Zn NPs functionalized with long PMOXA ligands remained stable for up to 9 months of incubation (see Table S2 in the Supporting Information).

Atomic force microscopy (AFM) tapping-mode micrographs qualitatively confirmed the results of DLS. As reported in Figure 5, the shorter PMOXA(18)ND and PMOXA(18)BrD

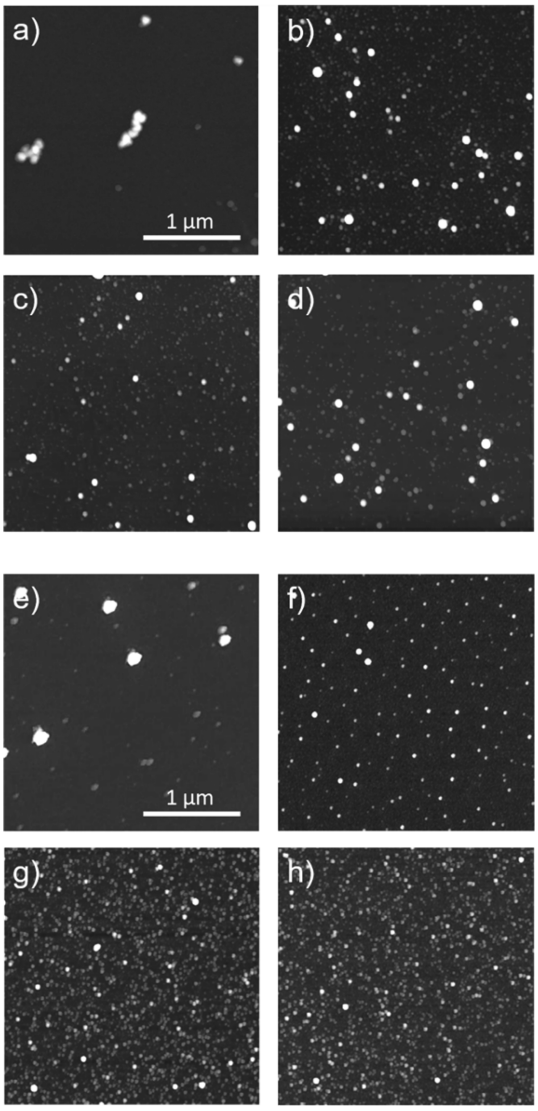

Figure 5. AFM tapping-mode micrographs showing ZnS NPs functionalized with (a–d) PMOXA(x)ND ligands and (e–h) PMOXA(x)BrD ligands: (a) ZnS:PMOXA(18)ND, (b) ZnS:PMOXA(27)ND, (c) ZnS:PMOXA(50)ND, (d) ZnS:PMOXA(90)ND, (e) ZnS:PMOXA(18)BrD, (f) ZnS:PMOXA(27)BrD, (g) ZnS:PMOXA(50)BrD, and (h) ZnS:PMOXA(90)BrD.

were not capable of providing singly dispersed NPs (see Figures 5a and 5e, for ZnS-PMOXA(18)ND and ZnS-PMOXA(18)BrD, respectively) from the native ZnS aggregates (Figure 3c), while NP clusters of variable size were found. In contrast, PMOXA ligands of higher DP produced fine dispersions of single NPs with average size in the range 50–100 nm (Figures 5b–d and 5f–h).

The different values of NP size provided by DLS, TEM, and AFM were probably due to the intrinsic differences in the physical quantities measured by these methods. Moreover, the increase in diameter recorded both by DLS, TEM, and AFM, compared to the crystallite size derived from XRD analysis, was

DOI: 10.1021/acs.langmuir.8b02287
Langmuir XXXX, XXX, XXX–XXX

ascribed to the steric hindrance provided by the dense PMOXA shells and their highly hydrated character.

The TEM-SAED micrographs reported in Figure 6 additionally highlighted the formation of an organic shell after

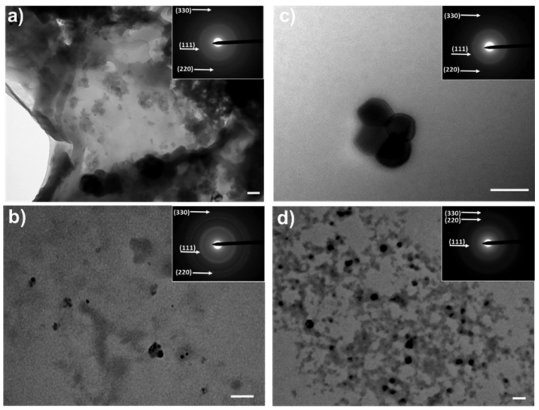

Figure 6. TEM micrographs and SAED pattern obtained from suspension of (a) ZnS-PMOXA(90)ND, (b) ZnS-PMOXA(90)BrD, (c) ZnS-PMOXA(27)BrD, and (d) ZnS-PMOXA(27)ND. All scale bars correspond to 100 nm.

functionalization of the pristine ZnS NPs with PMOXAND and PMOXABrD. The analysis of the corresponding diffraction patterns associated with the SAED analysis (insets in Figure 6a–d) further excluded the presence of ZnO on the NPs, confirming the presence of sulfides on the surface of the functionalized NPs.

Synthesis and Characterization of Tb-Doped ZnS-PMOXA NPs. In order to test their potential application as bioimaging probes, ZnS-PMOXA NPs were doped with Tb^{3+} as a luminescent component. Namely, ZnS:Tb NPs were synthesized by adding $Tb(NO_3)_3$ in a 1:20 Tb:Zn atomic ratio to the ME containing the Zn precursor.[22] ZnS:Tb NPs were functionalized in a similar way as already described for the ZnS NPs. XRD analyses (data not shown) proved the crystallization of sphalerite, irrespective of the presence of the inorganic dopant.

Phosphorescence emission spectroscopy confirmed the presence of Tb ions trapped in the ZnS nanostructures (see Figure 7a), through the strong, characteristic emission bands centered at 545, 594, and 625 nm.[62,63]

After ligand exchange, both ZnS:Tb-PMOXA(x)ND and ZnS:Tb-PMOXA(x)BrD showed a relevant decrease in phosphorescence intensity, with respect to the bare ZnS-Tb (Figure 7b), presumably due to absorption of the excitation wavelength by the ligands (Figure 7c). Nevertheless, this did not translate in a complete quenching of the signals, confirming that the NPs could be applied as imaging probes, even after PMOXA functionalization.

Cytotoxicity of ZnS-PMOXA NPs. In order to test the cytotoxicity and biocompatibility of the fabricated core–PMOXA shell NPs, human A549 cells were incubated for 24h in culture medium containing increasing concentrations of ZnS:Tb-PMOXA(x)ND and ZnS:Tb-PMOXA(x)BrD. The cytotoxicity of NPs was evaluated by clonogenic assay, which measures the ability of single cells to form colonies. This assay is based on the retention of proliferation ability by only viable and healthy cells. Therefore, it is a very sensitive test to assess the potential toxicity of NPs, with respect to common colorimetric assays, which, instead, are based on the detection of the cellular enzymatic activities.[57] The results showed that clonogenic cell survival is unaffected by incubation in ZnS:Tb-PMOXA NPs, highlighting that these are noncytotoxic at all of the concentrations tested (see Figure 8).

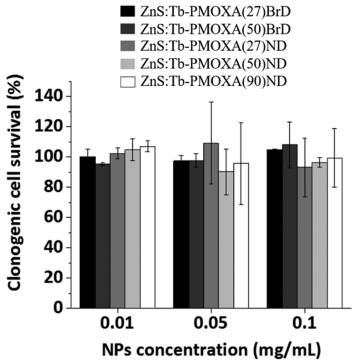

Figure 8. Cytotoxicity in human A549 cells. ZnS:Tb-PMOXA(x)ND and ZnS:Tb-PMOXA(x)Br. Cell survival was calculated as a percentage of cloning efficiency of NPs-treated cells over that of untreated control cells. Data are mean ± SD from three independent experiments.

In order to evaluate whether the NPs were efficiently internalized by the cells, the intracellular localization of ZnS:Tb-PMOXA(x)ND and ZnS:Tb-PMOXA(x)BrD NPs was analyzed by TEM. From the micrographs shown in Figure 9, the NPs were internalized by A549, and, even though they

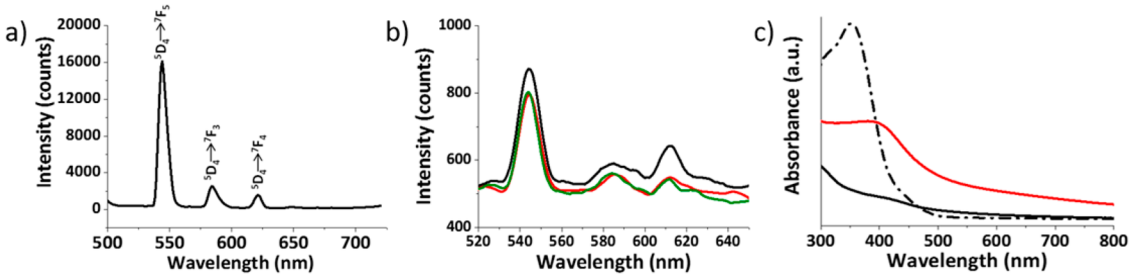

Figure 7. (a) Phosphorescence emission spectrum of ZnS:Tb, λ_{ex} = 487 nm. (b) Phosphorescence emission spectra of ZnS:Tb functionalized with three different PMOXA-based ligands: ZnS:Tb-PMOXA(50)ND (black trace), ZnS:Tb-PMOXA(90)ND (green trace), and ZnS:Tb-PMOXA(50)BrD (red trace). (c) Absorption spectra of ZnS:Tb-PMOXA(50)ND (red trace) and ZnS:Tb-PMOXA(27)BrD (black trace) in the visible wavelength range. The increased absorbance for ZnS:Tb-PMOXA(50)ND is ascribable to ND (dashed trace), while BrD does not absorb in the visible spectrum.

DOI: 10.1021/acs.langmuir.8b02287
Langmuir XXXX, XXX, XXX–XXX

accumulated in particular cell areas, they still maintained their individuality and did not aggregate.

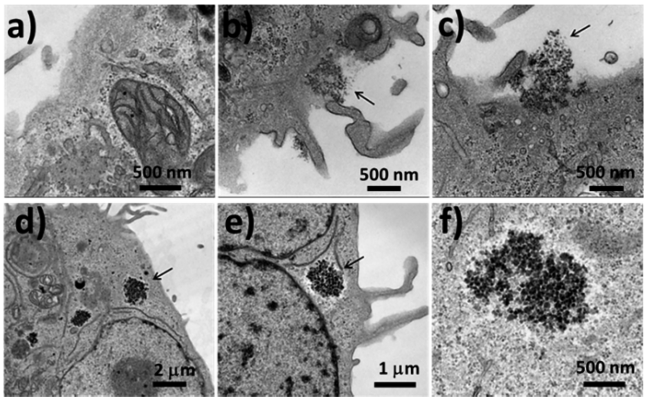

Figure 9. TEM micrographs showing the intracellular localization of ZnS:Tb-PMOXA(x)ND and ZnS:Tb-PMOXA(x)BrD NPs in A549 cells after 24 h of exposure. A549 control cells non incubated with NPs (panel (a)), and incubated with 0.2 mg mL^{-1} ZnS:Tb-PMOXA(27)BrD (panels (b) and (c)), or ZnS:Tb-PMOXA(50)ND (panels (d)−(f)). Arrows denote NPs.

CONCLUSIONS

In this work, we reported the successful preparation of ZnS and ZnS:Tb NPs via ME process and their subsequent, robust stabilization using cathecol-bearing PMOXA ligands of different molar masses. The inorganic NPs could be obtained as pure and highly crystalline compounds at room temperature. The combination of XRD, XPS, and TEM-SAED results allowed us to rule out the presence of oxide and sulfate passivation layers on the ZnS NPs. High-molar-mass PMOXA-based ligands ensured an efficient long-term stability of ZnS NP within water and PBS suspensions.. ZnS:Tb-PMOXAs were also proven to emit in the visible region of the spectrum and were tested in vitro, showing no detectable cytotoxicity. All these properties enable the application of these core−polymer shell NPs as novel inorganic labels for optical bioimaging.

ASSOCIATED CONTENT

Supporting Information

The Supporting Information is available free of charge on the ACS Publications website at DOI: 10.1021/acs.langmuir.8b02287.

Details regarding ME process, synthesis, and characterization of PMOXA ligands; DLS and TGA profiles of ZnS:PMOXAs NPs (PDF)

AUTHOR INFORMATION

Corresponding Authors

*Tel.: +39 049-8275736. E-mail: silvia.gross@unipd.it (S. Gross).

*Tel.: +41 (0)44 6326050. E-mail: edmondo.benetti@mat.ethz.ch (E. M. Benetti).

ORCID

Edmondo M. Benetti: 0000-0002-5657-5714

Silvia Gross: 0000-0003-1860-8711

Author Contributions

The manuscript was written through contributions of all authors and all authors have given approval to the final version of the manuscript.

Funding

This work was financially supported by the Swiss National Science Foundation (SNSF "Ambizione" PZ00P2−790 148156).

Notes

The authors declare no competing financial interest.

ACKNOWLEDGMENTS

We gratefully acknowledge Dr. Federico Caicci (Department of Biology, University of Padova) for TEM analyses. We thank Prof. Nicholas D. Spencer (ETH Zürich) for the precious scientific discussions and technical support.

REFERENCES

(1) Neouze, M.-A.; Schubert, U. Surface Modification and Functionalization of Metal and Metal Oxide Nanoparticles by Organic Ligands. *Monatsh. Chem.* **2008**, *139*, 183−195.

(2) Gross, S.; Vittadini, A.; Dengo, N. Functionalisation of Colloidal Transition Metal Sulphides Nanocrystals: A Fascinating and Challenging Playground for the Chemist. *Crystals* **2017**, *7*, 110.

(3) Mathew, M. E.; Mohan, J. C.; Manzoor, K.; Nair, S. V.; Tamura, H.; Jayakumar, R. Folate Conjugated Carboxymethyl Chitosan − Manganese Doped Zinc Sulphide Nanoparticles for Targeted Drug Delivery and Imaging of Cancer Cells. *Carbohydr. Polym.* **2010**, *80*, 442−448.

(4) Manzoor, K.; Johny, S.; Thomas, D.; Setua, S.; Menon, D.; Nair, S. Bio-Conjugated Luminescent Quantum Dots of Doped ZnS: A Cyto-Friendly System for Targeted Cancer Imaging. *Nanotechnology* **2009**, *20*, 065102.

(5) Greenwood, N. N.; Earnshaw, A. *Chemistry of the Elements*, 2nd Edition; Butterworth−Heinemann: Oxford, U.K., 1998.

(6) Holleman, A. F.; Wiberg, E.; Wiberg, N. *Lehrbuch Der Anorganischen Chemie*; de Gruyter: Berlin, 2007.

(7) Fang, X.; Zhai, T.; Gautam, U. K.; Li, L.; Wu, L.; Bando, Y.; Golberg, D. ZnS Nanostructures: From Synthesis to Applications. *Prog. Mater. Sci.* **2011**, *56*, 175−287.

(8) Yu, Z.; Ma, X.; Yu, B.; Pan, Y.; Liu, Z. Synthesis and Characterization of ZnS:Mn/ZnS Core/Shell Nanoparticles for Tumor Targeting and Imaging in Vivo. *J. Biomater. Appl.* **2013**, *28*, 232−240.

(9) Jayasree, A.; Sasidharan, S.; Koyakutty, M.; Nair, S.; Menon, D. Mannosylated Chitosan-Zinc Sulphide Nanocrystals as Fluorescent Bioprobes for Targeted Cancer Imaging. *Carbohydr. Polym.* **2011**, *85*, 37−43.

(10) Amaranatha Reddy, D.; Sambasivam, S.; Murali, G.; Poornaprakash, B.; Vijayalakshmi, R. P.; Aparna, Y.; Reddy, B. K.; Rao, J. L. Effect of Mn Co-Doping on the Structural, Optical and Magnetic Properties of ZnS:Cr Nanoparticles. *J. Alloys Compd.* **2012**, *537*, 208−215.

(11) Taherian, M.; Sabbagh Alvani, A. A.; Shokrgozar, M. A.; Salimi, R.; Moosakhani, S.; Sameie, H.; Tabatabaee, F. Surface-Treated Biocompatible ZnS Quantum Dots: Synthesis, Photo-Physical and Microstructural Properties. *Electron. Mater. Lett.* **2014**, *10*, 393−400.

(12) Hertl, W. Surface Chemical Properties of Zinc Sulfide. *Langmuir* **1988**, *4*, 594−598.

(13) Kezuka, T.; Konishi, M.; Isobe, T.; Senna, M. Preparation and Properties of Nanocrystalline ZnS: Mn-Polymer Composite ″ Lms. *J. Lumin.* **2000**, *87-89*, 418−420.

(14) Althues, H.; Palkovits, R.; Rumplecker, A.; Simon, P.; Sigle, W.; Bredol, M.; Kynast, U.; Kaskel, S.; et al. Synthesis and Characterization of Transparent Luminescent ZnS:Mn/PMMA Nanocomposites. *Chem. Mater.* **2006**, *18*, 1068−1072.

DOI: 10.1021/acs.langmuir.8b02287
Langmuir XXXX, XXX, XXX−XXX

(15) Kirchner, C.; Liedl, T.; Kudera, S.; Pellegrino, T.; Munoz Javier, A.; Gaub, H. E.; Stolzle, S.; Fertig, N.; Parak, W. J. Cytotoxicity of colloidal CdSe and CdSe/ZnS nanoparticles. *Nano Lett.* **2005**, *5*, 331−338.
(16) Finetti, C.; Colombo, M.; Prosperi, D.; Alessio, G.; Morasso, C.; Sola, L.; Chiari, M. One-Pot Phase Transfer and Surface Modification Functional Copolymer. *Chem. Commun.* **2014**, *50*, 240−242.
(17) Dey, S. K.; Sarkar, D. Effect of Zn Source Concentration on Structural, Optical and Electrical Properties of Zinc Sulphide−polyaniline (ZnS−PANI) Nanocomposite Thin Films. *J. Mater. Sci. Mater. Electron.* **2014**, *25*, 5638−5645.
(18) Wei, Y.; Yang, J.; Ying, J. Reversible Phase Transfer of Quantum Dots and Metal Nanoparticles. *Chem. Commun.* **2010**, *46*, 3179−3181.
(19) Yu, X.; Lei, D. Y.; Amin, F.; Hartmann, R.; Acuna, G. P.; Guerrero-Martínez, A.; Maier, S. A.; Tinnefeld, P.; Carregal-Romero, S.; Parak, W. J. Distance Control In-between Plasmonic Nanoparticles via Biological and Polymeric Spacers. *Nano Today* **2013**, *8*, 480−493.
(20) Augustine, M. S.; Anas, A.; Das, A. V.; Sreekanth, S.; Jayalekshmi, S. Spectrochimica Acta Part A: Molecular and Biomolecular Spectroscopy Cytotoxicity and Cellular Uptake of ZnS: Mn Nanocrystals Biofunctionalized with Chitosan and Amino-acids. *Spectrochim. Acta A* **2015**, *136*, 327−333.
(21) Singhal, M.; Sharma, J. K.; Jeon, H. C.; Kang, T. W.; Kumar, S. Effect of Pyridine Capping on Morphological and Optical Properties of ZnS:Mn2+ Core−shell Quantum Dots. *J. Mater. Sci. Mater. Electron.* **2016**, *27*, 3003−3010.
(22) Jain, A.; Jain, A.; Panwar, S.; Singh, R.; Singhal, M.; Sharma, J. K.; Ahuja, R.; Jeon, H. C.; Kang, T. W.; Kumar, S. Studies of Hypro-Mellose (HPMC) Functionalized ZnS:Mn Fluorescent Quantum Dots. *J. Mater. Sci. Mater. Electron.* **2017**, *28*, 1931−1937.
(23) Morgese, G.; Benetti, E. M. Polyoxazoline Biointerfaces by Surface Grafting. *Eur. Polym. J.* **2017**, *88*, 470−485.
(24) Hoogenboom, R. Poly(2-Oxazoline)s: Alive and Kicking. *Macromol. Chem. Phys.* **2007**, *208*, 18−25.
(25) Sedlacek, O.; Monnery, B. D.; Filippov, S. K.; Hoogenboom, R.; Hruby, M. Poly(2-Oxazoline)s-Are They More Advantageous for Biomedical Applications than Other Polymers? *Macromol. Rapid Commun.* **2012**, *33*, 1648−1662.
(26) Hoogenboom, R. Poly(2-Oxazoline)s: A Polymer Class with Numerous Potential Applications. *Angew. Chem. Int. Ed.* **2009**, *48*, 7978−7994.
(27) Adams, N.; Schubert, U. S. Poly(2-Oxazolines) in Biological and Biomedical Application Contexts. *Adv. Drug Delivery Rev.* **2007**, *59*, 1504−1520.
(28) Herold, D. A.; Keil, K.; Bruns, D. E. Oxidation of Polyethylene Glycols by Alcohol Dehydrogenase. *Biochem. Pharmacol.* **1989**, *38*, 73−76.
(29) Ostuni, E.; Chapman, R. G.; Holmlin, R. E.; Takayama, S.; Whitesides, G. M. A Survey of Structure-Property Relationships of Surfaces That Resist the Adsorption of Protein. *Langmuir* **2001**, *17*, 5605−5620.
(30) Konradi, R.; Pidhatika, B.; Mühlebach, A.; Textor, M. Poly-2-Methyl-2-Oxazoline: A Peptide-like Polymer for Protein-Repellent Surfaces. *Langmuir* **2008**, *24*, 613−616.
(31) Konradi, R.; Acikgoz, C.; Textor, M. Polyoxazolines for Nonfouling Surface Coatings - A Direct Comparison to the Gold Standard PEG. *Macromol. Rapid Commun.* **2012**, *33*, 1663−1676.
(32) Luxenhofer, R.; Sahay, G.; Schulz, A.; Alakhova, D.; Bronich, T. K.; Jordan, R.; Kabanov, A. V. Structure-Property Relationship in Cytotoxicity and Cell Uptake of Poly (2-Oxazoline) Amphiphiles. *J. Control. Release* **2011**, *153*, 73−82.
(33) Bauer, M.; Schroeder, S.; Tauhardt, L.; Kempe, K.; Schubert, U. S.; Fischer, D. In Vitro Hemocompatibility and Cytotoxicity Study of Poly (2-methyl-2-oxazoline) for Biomedical Applications. *J. Polym. Sci.A* **2013**, *51*, 1816−1821.
(34) Ulbricht, J.; Jordan, R.; Luxenhofer, R. On the Biodegradability of Polyethylene Glycol, Polypeptoids and Poly(2-Oxazoline)S. *Biomaterials* **2014**, *35*, 4848−4861.
(35) Morgese, G.; Causin, V.; Maggini, M.; Corrà, S.; Gross, S.; Benetti, E. M. Ultrastable Suspensions of Polyoxazoline-Functionalized ZnO Single Nanocrystals. *Chem. Mater.* **2015**, *27*, 2957−2964.
(36) Morgese, G.; Shirmardi Shaghasemi, B.; Causin, V.; Zenobi-Wong, M.; Ramakrishna, S. N.; Reimhult, E.; Benetti, E. M. Next-Generation Polymer Shells for Inorganic Nanoparticles Are Highly Compact, Ultra-Dense, and Long-Lasting Cyclic Brushes. *Angew. Chem. Int. Ed.* **2017**, *56*, 4507−4511.
(37) Gal, N.; Schroffenegger, M.; Reimhult, E. Stealth Nanoparticles Grafted with Dense Polymer Brushes Display Adsorption of Serum Protein Investigated by Isothermal Titration Calorimetry. *J. Phys. Chem. B* **2018**, *122*, 5820−5834.
(38) Dolcet, P.; Maurizio, C.; Casarin, M.; Pandolfo, L.; Gialanella, S.; Badocco, D.; Pastore, P.; Speghini, A.; Gross, S. An Effective Two-Emulsion Approach to the Synthesis of Doped ZnS Crystalline Nanostructures. *Eur. J. Inorg. Chem.* **2015**, *2015*, 706−714.
(39) Xu, C.; Xu, K.; Gu, H.; Zheng, R.; Liu, H.; Zhang, X.; Guo, Z.; Xu, B. Dopamine as a Robust Anchor to Immobilize Functional Molecules on the Iron Oxide Shell of Magnetic Nanoparticles. *J. Am. Chem. Soc.* **2004**, *126*, 9938−9939.
(40) Amstad, E.; Gillich, T.; Bilecka, I.; Textor, M.; Reimhult, E. Ultrastable Iron Oxide Nanoparticle Colloidal Suspensions Using Dispersants with Catechol-Derived Anchor Groups. *Nano Lett.* **2009**, *9*, 4042−4048.
(41) Zhang, Q.; Nurumbetov, G.; Simula, A.; Zhu, C. Y.; Li, M. X.; Wilson, P.; Kempe, K.; Yang, B.; Tao, L.; Haddleton, D. M. Synthesis of well-defined catechol polymers for surface functionalization of magnetic nanoparticles. *Polym. Chem.* **2016**, *7*, 7002−7010.
(42) Shultz, M. D.; Reveles, J. U.; Khanna, S. N.; Carpenter, E. E. Reactive nature of dopamine as a surface functionalization agent in iron oxide nanoparticles. *J. Am. Chem. Soc.* **2007**, *129*, 2482−2487.
(43) Napolitano, A.; D'Ischia, M.; Costantini, C.; Prota, G. A New Oxidation Pathway of the Neurotoxin Isolation and Characterisation of a Dimer with A. *Tetrahedron* **1992**, *48*, 8515−8522.
(44) Filer, C. N.; Orphanos, D.; Seguin, R. J. Synthesis of [Ring- 3 H] Dopamine and Fluoro Analogues at High Specific Activity. *Synth. Commun.* **2006**, *36*, 975−978.
(45) Shevchenko, V. P.; Nagaev, I. Y.; Shevchenko, K. V.; Chernysheva, M. G.; Badun, G. a.; Fedoseev, V. M.; Myasoedov, N. F. Solid-Phase Synthesis of Deuterium- and Tritium-Labeled Dopamine Using Carbon Nanomaterials. *Radiochemistry* **2011**, *53*, 336−340.
(46) Muñoz-Espí, R.; Weiss, C. K.; Landfester, K. Inorganic Nanoparticles Prepared in Miniemulsion. *Curr. Opin. Colloid Interface Sci.* **2012**, *17*, 212−224.
(47) Muñoz-Espí, R.; Mastai, Y.; Gross, S.; Landfester, K. Colloidal Systems for Crystallization Processes from Liquid Phase. *CrystEng-Comm* **2013**, *15*, 2175.
(48) Harmer, S. L.; Goncharova, L. V.; Kolarova, R.; Lennard, W. N.; Muñoz-Márquez, M. a.; Mitchell, I. V.; Nesbitt, H. W. Surface Structure of Sphalerite Studied by Medium Energy Ion Scattering and XPS. *Surf. Sci.* **2007**, *601*, 352−361.
(49) Fede, C.; Selvestrel, F.; Compagnin, C.; Mognato, M.; Mancin, F.; Reddi, E.; Celotti, L. The Toxicity Outcome of Silica Nanoparticles (Ludox ®) Is Influenced by Testing Techniques and Treatment Modalities. *Anal. Bioanal. Chem.* **2012**, *404*, 1789−1802.
(50) Compagnin, C.; Mognato, M.; Celotti, L.; Canti, G.; Palumbo, G.; Reddi, E. Cell Proliferation and Cell Cycle Alterations in Oesophageal P53-Mutated Cancer Cells Treated with Cisplatin in Combination with Photodynamic Therapy. *Cell Prolif.* **2010**, *43*, 262−274.
(51) Hecht, F. M.; Bausch, A. R. Kinetically Guided Colloidal Structure Formation. *Proc. Natl. Acad. Sci. U.S.A.* **2016**, *113*, 8577−8582.

DOI: 10.1021/acs.langmuir.8b02287
Langmuir XXXX, XXX, XXX−XXX

(52) Landfester, K. Miniemulsion Polymerization and the Structure of Polymer and Hybrid Nanoparticles. *Angew. Chem. Int. Ed.* **2009**, *48*, 4488−4507.
(53) Montenegro, R.; Antonietti, M.; Mastai, Y.; Landfester, K. Crystallization in Miniemulsion Droplets. *J. Phys. Chem. B* **2003**, *107*, 5088−5094.
(54) Landfester, K. Miniemulsions for Nanoparticle Synthesis. *Top. Curr. Chem.* **2003**, *227*, 75−123.
(55) Landfester, K. The Generation of Nanoparticles in Miniemulsions. *Adv. Mater.* **2001**, *13*, 765−768.
(56) Dolcet, P.; Casarin, M.; Maccato, C.; Bovo, L.; Ischia, G.; Gialanella, S.; Mancin, F.; Tondello, E.; Gross, S. Miniemulsions as Chemical Nanoreactors for the Room Temperature Synthesis of Inorganic Crystalline Nanostructures: ZnO Colloids. *J. Mater. Chem.* **2012**, *22*, 1620.
(57) Dolcet, P.; Mambrini, A.; Pedroni, M.; Speghini, A.; Gialanella, S.; Casarin, M.; Gross, S. Room Temperature Crystallization of Highly Luminescent Lanthanide-Doped CaF_2 in Nanosized Droplets: First Example of the Synthesis of Metal Halogenide in Miniemulsion with Effective Doping and Size Control. *RSC Adv.* **2015**, *5*, 16302−16310.
(58) Dolcet, P.; Latini, F.; Casarin, M.; Speghini, A.; Tondello, E.; Foss, C.; Diodati, S.; Verin, L.; Motta, A.; Gross, S. Inorganic Chemistry in a Nanoreactor: Doped ZnO Nanostructures by Miniemulsion. *Eur. J. Inorg. Chem.* **2013**, *2013*, 2291−2300.
(59) Scherrer, P. Bestimmung Der Grosse Und Der Inneren Struktur von Kolloidteilchen Mittels Rontgenstrahlen, Nachrichten von Der Gesellschaft Der Wissenschaften. *Math. Phys. Klasse* **1918**, *2*, 98−100.
(60) Moulder, J. M. F.; Stickle, W. F.; Sobol, P. E.; Bomben, K. D. *Handbook of X-ray Photoelectron Spectroscopy*; Perkin−Elmer Corporation: Eden Prairie, MN, 1992.
(61) Naumkin, A. V; Kraut-Vass, A.; Gaarenstroom, S. W.; Powell, C. J. *NIST X-ray Photoelectron Spectroscopy Database*; National Institutes of Science and Technology: Gaithersburg, MD.
(62) Bhargava, R. N. Doped Nanocrystalline Materials — Physics and Applications. *J. Lumin.* **1996**, *70*, 85−94.
(63) Shirley, D. A. High-Resolution x-Ray Photoemission Spectrum of the Valence Bands of Gold. *Phys. Rev. B* **1972**, *5*, 4709−4714.

DOI: 10.1021/acs.langmuir.8b02287
Langmuir XXXX, XXX, XXX−XXX